

# Towards Adversarially Robust Deepfake Detection: An Ensemble Approach

Ashish Hooda<sup>\*,1</sup>      Neal Mangaokar<sup>\*,2</sup>      Ryan Feng<sup>2</sup>  
Kassem Fawaz<sup>1</sup>      Somesh Jha<sup>1</sup>      Atul Prakash<sup>2</sup>

<sup>1</sup>{ahooda, kfawaz, jha}@wisc.edu  
<sup>2</sup>{nealmgkr, rtfeng, aprakash}@umich.edu

## Abstract

Detecting deepfakes is an important problem, but recent work has shown that DNN-based deepfake detectors are brittle against *adversarial deepfakes*, in which an adversary adds imperceptible perturbations to a deepfake to evade detection. In this work, we show that a modification to the detection strategy in which we replace a single classifier with a carefully chosen ensemble, in which input transformations for each model in the ensemble induces pairwise orthogonal gradients, can significantly improve robustness beyond the *de facto* solution of adversarial training. We present theoretical results to show that such orthogonal gradients can help thwart a first-order adversary by reducing the dimensionality of the input subspace in which adversarial deepfakes lie. We validate the results empirically by instantiating and evaluating a randomized version of such “orthogonal” ensembles for adversarial deepfake detection and find that these randomized ensembles exhibit significantly higher robustness as deepfake detectors compared to state-of-the-art deepfake detectors against adversarial deepfakes, even those created using strong PGD-500 attacks.

## 1 Introduction

Significant advances in deep-learning are responsible for the advent of “deepfakes”, which broadly refer to digital media that has been synthetically generated/modified by a deep neural network (DNN). Specifically, modern DNNs such as generative adversarial networks (GANs) [1] and auto-encoders [2]

---

\* Indicates equal contribution.

are now capable of crafting hyper-realistic images and videos that are indistinguishable from real content. This has led to a rising concern of bad actors that can misuse deepfakes to craft fake social media profiles [3], illicit pornography [4], spread political propaganda, and even manipulate elections.

In response to these concerns, recent work has attempted to solve the deepfake detection problem, in which a defender attempts to classify given media as deepfake or real. These detection schemes often leverage DNNs themselves [5]. Unfortunately, it has been shown that DNN-based defenses are vulnerable to further adaptive attacks, i.e., adversarial examples [6, 7, 8]. For example, Carlini et al. [9] successfully evade detection against Frank et al.’s [5] state-of-the-art frequency-space DNN defense by flipping the lowest bit in each pixel of deepfake images. Similar efforts by Neekhara et al. [10] and others corroborate this vulnerability.

One approach to increasing robustness is to use an ensemble of models. However, simple applications of ensembles have been shown to be a broken defense [11]. More recent work attributes this to adversarial examples transferring between individual models, often counteracted by adding additional loss terms to reduce gradient similarity via “orthogonal gradients” [12, 13].

Our first key observation is that we can achieve gradient orthogonality directly through cleverly chosen input transformations, removing the need for additional training objectives. Specifically, we show in Section 3.2 that using affine input transformation matrices to orthogonal subspaces induces pairwise orthogonal gradients. We then demonstrate and empirically confirm in Sections 3.3 and 4.2.1 respectively that appropriately chosen input bases in conjunction with these transformation functions can induce gradient orthogonality without affecting classification performance.

Our second key observation is that orthogonal gradients can reduce the dimensionality of the subspace of adversarial examples for an ensemble, thereby reducing the attack surface. Specifically, we extend Tramer et al.’s results [14, 15] in Section 3.1 to provide new theoretical bounds on the maximum number of adversarial directions that can be found, in terms of the angles between gradients. We then empirically estimate the size of the adversarial subspace with these orthogonal directions in Section 4.2.2, giving a theoretically-backed result to demonstrate the reduction of the attack space.

Finally, we instantiate these ideas to improve adversarial robustness in the context of deepfake detection. To this end, we employ ensembles comprising frequency spectrum-based DNN classifiers to detect images generated from the state-of-the-art StyleGAN [16] model. Each model in our ensembles leverages a partition of frequency components to satisfy our goal of creating

orthogonal gradients. On pools of ensembles using as few as 12.5% of frequency components, we find that our ensembles are more robust than the baseline DNN deepfake classifier proposed by Frank et al. [5]. We evaluate on adaptively designed PGD-500 attacks and find that randomized versions of our ensembles can achieve adversarial accuracies of up to  $\sim 70\%$  compared to 0% for the baseline, demonstrating a practical instantiation of attack surface reduction through orthogonal gradients.

Our contributions can be summarized as follows:

1. We present a novel framework of defenses that build robust ensembles with orthogonal gradients through the construction of orthogonal subspaces in pre-processing.
2. We prove new bounds on the maximum number of adversarial directions that can be found under such an ensemble, thereby reducing expected dimensionality of the adversarial subspace.
3. We present an adversarially robust deepfake defense based on the above principles by using ensembles of frequency spectrum-based deepfake classifiers, achieving up to  $\sim 70\%$  adversarial robustness against PGD-500 vs. 0% on the baseline.

## 2 Background and Related Work

### 2.1 Notation

We assume a distribution  $\mathcal{D}$  over  $\mathcal{X} \times \mathcal{Y}$ , where  $\mathcal{X} \in \mathbb{R}^d$  is the input space and  $\mathcal{Y} \in \mathbb{Z}$  is the finite class-label space. We denote vectors in boldface (e.g.  $\mathbf{x}$ ). We denote a trained classifier as  $\mathcal{F} : \mathcal{X} \rightarrow \mathcal{Y}$  (the classifier is usually parameterized by its weights  $w$ , but we will omit it for brevity). We denote the loss function as  $\mathcal{L}(\mathbf{x}, y)$ .

### 2.2 GANs and Deepfakes

Deepfakes broadly refer to digital media generated/modified by a DNN. In this work, we focus on deepfake images generated by the GAN family of DNNs. A GAN comprises a pair of networks — a generator  $\mathcal{G}$  and discriminator  $\mathcal{D}$ . These networks are trained in tandem with one another, i.e.,  $\mathcal{G}$  learns to generate realistic images from input space  $\mathcal{X}$ , and the  $\mathcal{D}$  learns to provide  $\mathcal{G}$  with feedback regarding the quality of generated images,

so that it may improve. Recent work has significantly advanced the state-of-the-art for GANs [17, 16, 18, 19, 20, 21], thereby enabling the generation of hyper-realistic deepfake images.

### 2.3 Deepfake Detection

The research community has made significant progress towards detecting deepfake images. Examples of proposed detection schemes have included ordinary DNN classifiers [22, 23] color-space anomaly detection [24], and co-occurrence matrix analysis [25].

More recent work has advanced the state-of-the-art for deepfake detection by leveraging frequency-space analysis. For example, Frank et al. [5] proposed the use of DNNs to detect deepfakes, but with the Discrete Cosine Transform (DCT) as a pre-processing transform. Their findings suggest that the upsampling processes used in GAN image generation often leave behind extensive frequency domain artifacts. Their observations have been corroborated by similar work — Zhang et al. [26] have used GAN simulators to extract similar frequency artifacts, and Durall et al. [27] have also successfully trained DNNs in the frequency domain to detect deepfakes.

### 2.4 Adversarial Examples

For a classifier  $\mathcal{F}$  and an input-label pair  $(\mathbf{x}, y)$ , an adversarial example is a perturbed input  $\mathbf{x}'$  such that (1)  $\mathbf{x}$  is mis-classified i.e.  $\mathcal{F}(\mathbf{x}') \neq y$  and (2)  $\|x - x'\|$  is small, where  $\|\cdot\|$  is some norm.

As such, many DNN-based image classifiers have been shown to be vulnerable to adversarial examples [8, 7, 6]. In fact, recent work from Carlini and Farid [9] has shown that with as little as the ability to flip the lowest bit in each pixel, deepfake images can be attacked to evade detection by modern DNN deepfake detection classifiers (e.g., those from Frank et al. [5] and Wang et al. [22]). Neekhara et al. [10] have also explored black-box attacks and Universal Adversarial Perturbation [28] style attacks on deepfake detection.

### 2.5 Defenses Against Adversarial Examples

#### 2.5.1 Ensemble Defenses and Transferability Shortcoming

An ensemble classifier is a function  $E_{(\mathcal{F}_1, \mathcal{F}_2, \dots, \mathcal{F}_n)} : \mathcal{X} \rightarrow \mathcal{Y}$  that combines the logit outputs  $\ell_1, \ell_2, \dots, \ell_n$  of the multiple classifiers  $\mathcal{F}_1, \mathcal{F}_2, \dots, \mathcal{F}_n$  with a voting aggregation function  $\mathcal{A}_{(\ell_1, \ell_2, \dots, \ell_n)} : \mathbb{R}^{|\mathcal{Y}|} \rightarrow \mathcal{Y}$ , such as averaging.

The idea of ensemble-based defenses to defend against adversarial examples has been previously explored, with the idea being that it is harder to break multiple models than just one. However, He et al. [11] initially showed that ensembling weak defenses does not necessarily lead to robust defenses. One difficulty with ensembles is that of *transferability shortcoming*, i.e., adversarial examples are often found to transfer between two individual models in the ensemble [29], especially for models with high dimensionality of the adversarial subspace [14].

### 2.5.2 Adversarial Training

A widely accepted solution to adversarial examples is to adversarially train the model. Adversarial training, as first proposed by Madry et al. [30], entails training the DNN on the adversarial examples themselves. However, Carlini et al. [9] suggest that adversarial training alone is unlikely to achieve significant improvement in robustness in the more difficult deepfake setting – a stronger attack than used in adversarial training can usually fully bypass the defense. For instance, our experiments in Section 4 confirm that Frank et al.’s deepfake detector, when adversarially trained using de facto PGD-10 adversarial examples, is entirely susceptible to evasion by deepfake examples that were slightly modified using a PGD-100 attack on the adversarially-trained Frank et al.’s deepfake detector.

## 3 Proposed Approach: Robust Ensembles via Gradient Orthogonality

As noted in the previous section, an attacker typically targets the classifier through solving an optimization problem that elicits classification errors. An ensemble presents an attractive defense option by introducing multiple constraints to the optimization problem that the attacker must solve to find a successful attack. However, the ensemble needs to avoid the transferability shortcoming noted earlier. In particular, the different models comprising the ensemble often share the adversarial subspace; an adversarial example that is successful against one model is likely to be successful against other models, especially for models with high dimensionality of the adversarial subspace [14]. We extend this work to characterize the dimensionality of the adversarial subspace of an ensemble of models and find it depending on two factors: (1) the similarity between the gradients of the models and (2) the magnitudes of the gradients.

In what follows, we elaborate on our characterization of the dimensionality of the adversarial subspace and how this characterization enables the design of a more robust ensemble of models for detecting deepfakes.

### 3.1 Dimensionality of Shared Adversarial Subspace

To fool an ensemble based defense, an adversarial example needs to be adversarial for each of the constituent classifiers. For an ensemble of two classifiers -  $\mathcal{F}$  and  $\mathcal{G}$ , the subspace of adversarial examples is the intersection of adversarial subspaces for both the models i.e. the shared adversarial subspace.

For a single model  $\mathcal{F}$  and input  $\mathbf{x}$ , Tramer et al. [14] formalize the  $k$ -dimensional adversarial subspace as the span of orthogonal perturbations  $\mathbf{r}_1, \dots, \mathbf{r}_k \in \mathbb{R}^d$  where  $\|\mathbf{r}_i\|_2 \leq \epsilon$  and  $\mathbf{r}_i^T \nabla_{\mathbf{x}} \mathcal{L}_{\mathcal{F}}(\mathbf{x}, y) \geq \gamma$ , where  $\mathcal{L}_{\mathcal{F}}$  is the loss function used to train  $\mathcal{F}$  and  $\gamma$  is the increase in loss sufficient to cause a mis-classification.

Note that an upper bound on  $k$  for a single classifier  $\mathcal{F}$  implicitly establishes a trivial upper bound on dimensionality of the shared subspace between  $\mathcal{F}$  and a second model  $\mathcal{G}$ . Tramer et al. [14] derive a closed form expression for this bound as  $\frac{\epsilon^2 \|\nabla_{\mathbf{x}} \mathcal{L}_{\mathcal{F}}(\mathbf{x}, y)\|_2^2}{\gamma^2}$ . We begin by extending this result to an upper bound on dimensionality of the shared adversarial subspace between  $n$  models.

**Lemma 3.1.** *Given  $n$  models,  $\mathcal{F}_1, \dots, \mathcal{F}_n$ , having gradients  $\mathbf{g}_1, \dots, \mathbf{g}_n \in \mathbb{R}^d$  for input-label pair  $(\mathbf{x}, y)$  (where  $\mathbf{g}_j = \nabla_{\mathbf{x}} \mathcal{L}_{\mathcal{F}_j}(\mathbf{x}, y)$ ), the maximum number  $k$  of orthogonal vectors  $\mathbf{r}_1, \mathbf{r}_2, \dots, \mathbf{r}_k \in \mathbb{R}^d$  satisfying  $\|\mathbf{r}_i\|_2 \leq \epsilon$  and  $\mathbf{r}_i^T \mathbf{g}_j \geq \gamma_j$  for all  $1 \leq i \leq k$  and  $1 \leq j \leq n$  is given by:*

$$k \leq \min(k_{ind}, k_{sim}, d)$$

$$\text{where, } k_{ind} = \min_{1 \leq j \leq n} \frac{\epsilon^2}{\gamma_j^2} \|\mathbf{g}_j\|_2^2$$

$$k_{sim} = \frac{\epsilon^2}{\left(\sum_{j=1}^n \gamma_j\right)^2} \left( \sum_{j=1}^n \|\mathbf{g}_j\|_2^2 + \sum_{j_1=1}^n \sum_{j_2=1}^n \mathbf{g}_{j_1}^T \mathbf{g}_{j_2} \right)$$

Here,  $\gamma_j$  is the increase in loss sufficient to cause a mis-classification for classifier  $\mathcal{F}_j$  i.e.  $\mathcal{F}_j(\mathbf{x}) \neq y$ . The proof is provided in Appendix A. Note that  $k_{ind}$  is the trivial case, as the dimension of the intersection cannot exceed the dimension of any of the individual model's adversarial subspace. We also observe that the bound is further minimized when an ensemble

satisfies two key properties: (1) models have near-identical gradient norms and distances to the decision boundaries i.e.,  $\|\mathbf{g}_1\|_2 \approx \|\mathbf{g}_2\|_2 \approx \dots \approx \|\mathbf{g}_n\|_2$  and  $\gamma_1 \approx \gamma_2 \approx \dots \approx \gamma_k$ . (2) models have pairwise orthogonal gradients (reducing the dot products in  $k_{sim}$  to 0). When (1) and (2) are satisfied, then  $k_{sim} = \frac{k_{ind}}{n}$ , which reduces the upper bound by a factor of  $n$ .

We leverage this result to propose an ensemble design that satisfies the above two properties and achieves this reduced upper bound. First, we achieve model similarity by adversarially training the constituent classifiers with identical architectures, datasets, and hyperparameters.

Second, we carefully craft our ensembles to have orthogonal gradients by design, removing the need for additional training objectives while still increasing robustness. We do so by cleverly choosing pre-processing transformations such as using disjoint DCT regions that enforce orthogonal gradients. This approach obviates the need for additional training objectives to enforce gradient diversity as has been proposed earlier [12, 13].

### 3.2 Orthogonal Gradients using Transformations

Next, we find the necessary condition for a set of  $n$  transformation (for each of the constituent models) that ensures pairwise orthogonality of model gradients. Given input space  $\mathcal{X}$  and class-label space  $\mathcal{Y}$ , let  $\mathcal{V}_1, \dots, \mathcal{V}_n$  be vector spaces induced by affine transformations such that

$$\mathbf{v}_i = T_i \mathbf{x}$$

where  $\mathbf{v}_i \in \mathcal{V}_i, \mathbf{x} \in \mathcal{X}$ . Now, for  $n$  classifier functions  $\mathcal{F}_1, \dots, \mathcal{F}_n$ , where  $\mathcal{F}_i : \mathbf{v}_i \rightarrow y$ , that are trained using loss functions  $\mathcal{L}_{\mathcal{F}_1}, \dots, \mathcal{L}_{\mathcal{F}_n}$  respectively, for all  $1 \leq i \leq n$  we have,

$$\frac{\partial \mathcal{L}_{\mathcal{F}_i}(\mathbf{v}_i, y)}{\partial \mathbf{x}} = T_i^\top \frac{\partial \mathcal{L}_{\mathcal{F}_i}(\mathbf{v}_i, y)}{\partial \mathbf{v}_i}$$

using the chain rule. Now the dot product between the gradient of classifiers  $\mathcal{F}_i$  and  $\mathcal{F}_j$ , given as:

$$\begin{aligned} (\nabla_{\mathbf{x}} \mathcal{L}_{\mathcal{F}_i})^\top (\nabla_{\mathbf{x}} \mathcal{L}_{\mathcal{F}_j}) &= (\nabla_{\mathbf{v}_i} \mathcal{L}_{\mathcal{F}_i})^\top T_i T_j^\top (\nabla_{\mathbf{v}_j} \mathcal{L}_{\mathcal{F}_j}) \\ &\leq \|\nabla_{\mathbf{v}_i} \mathcal{L}_{\mathcal{F}_i}\|_2 \|\nabla_{\mathbf{v}_j} \mathcal{L}_{\mathcal{F}_j}\|_2 \sum_{(p,q)} |(T_i T_j^\top)_{pq}| \end{aligned}$$

Note  $\sum_{(p,q)} |(T_i T_j^\top)_{pq}|$  (sum of absolute values of all entries in  $T_i T_j^\top$ ) is zero for all  $i, j$  when  $\mathcal{V}_1, \dots, \mathcal{V}_n$  are pairwise orthogonal subspaces. In that

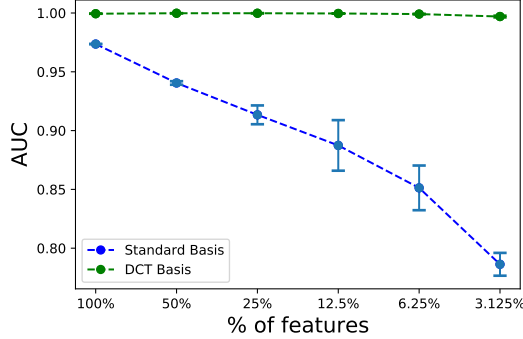


Figure 1: AUC-ROC scores of classifiers looking at smaller partitions of the input basis.

case,  $\mathcal{F}_1, \dots, \mathcal{F}_n$  have loss gradients that are pairwise orthogonal at all inputs. We can then leverage these transformations to build an ensemble of models with orthogonal gradients.

### 3.3 Constructing a Robust Ensemble

Using the above result, we now propose an ensemble design where constituent models look at pairwise orthogonal feature subspaces.

Let  $\mathcal{B} = \{\mathbf{b}_1, \dots, \mathbf{b}_d\}$  be an orthogonal basis for the input space  $\mathcal{X} \in \mathbb{R}^d$ . To split  $\mathcal{X}$  into pairwise orthogonal subspaces, we generate  $n$  (where  $n \leq d$ ) partitions of  $\mathcal{B}$ :  $B_1, \dots, B_n$  such that  $B_i \cap B_j = \emptyset \ \forall \ i \neq j$ . Then,  $\text{span}(B_1), \dots, \text{span}(B_n)$  are mutually orthogonal.

Additionally, if these partitions are sampled uniformly at random such that  $|B_i| = |B_j| \ \forall \ 1 \leq i, j \leq n$ , then models receive roughly “equivalent” subspaces. Assuming identical architectures, datasets, and hyperparameters, these models should then be near-identical.

Let  $T_1, \dots, T_n$  be the corresponding orthogonal projections, where  $T_i : \mathcal{X} \rightarrow \text{span}(B_i)$ . Now, we construct an ensemble of  $n$  classifiers  $E_{(\mathcal{F}_1, \mathcal{F}_2, \dots, \mathcal{F}_n)} : \mathcal{X} \rightarrow \mathcal{Y}$  where

$$\mathcal{F}_i : T_i(\mathcal{X}) \rightarrow \mathcal{Y}$$

Note that this design could hypothetically be applied to any classification problem. In the context of deepfake detection, we select basis  $\mathcal{B}$  for our input space to be the cosine basis functions associated with the frequency space induced by the Discrete Cosine Transform (DCT). This choice of basis and input space are motivated by prior work from Frank et al. [5] —

when transformed to the frequency space, deepfake images exhibit artifacts *throughout* the frequency spectrum. This allows us to adopt our orthogonality-inducing partitioning scheme without impacting performance.

## 4 Experimental Evaluation

In the following, we detail experiments used to evaluate the utility and robustness properties of the aforementioned ensembles. We consider an adversarially trained version of Frank et al.’s [5] frequency-space deepfake classifier (i.e., single model, no partitioning) as our baseline. Our experiments broadly aim to answer the following questions:

**Q1.** What is the classification performance of orthogonal ensembles in comparison to a single classifier?

**A1.** With an appropriately chosen basis, orthogonal ensembles exhibit performance comparable to that of a single classifier. We observe maximum reductions of  $< 1\%$  in AUC-ROC score even for ensembles of size  $n = 8$ . This performance can be attributed to the choice of DCT-induced frequency space — ensembles with partitioning in the pixel space suffer from drops of  $\sim 7\%$  in scores.

**Q2.** Do these ensembles reduce the dimensionality of the adversarial subspace? If so, how does size of the ensemble (i.e., the number of orthogonal constraints for the adversary) affect the attack surface?

**A2.** Increasing ensemble size increases the number of orthogonal constraints on the adversary’s optimization — we observe that ensembles of size  $n = 8$  exhibit  $\sim 0$  expected adversarial directions, in comparison to  $\sim 26$  for an ensemble of size  $n = 1$ . In fact, maximally sized versions of our ensembles demonstrate reductions down to  $\sim 0\%$  probability of finding any adversarial directions, in comparison to  $\sim 30\%$  probability for the baseline. In other words, our orthogonal ensembles reduce the number of discoverable adversarial directions for a single-step first-order adversary.

**Q3.** How well do these ensembles fare against an adaptive first-order adversary with increasingly large perturbation and computational budgets?

**A3.** Orthogonal ensembles offer significant robustness against a multi-step first-order adversary. Even under adaptive versions of PGD-500 for ensembles (with a perturbation budget  $\epsilon = 1/255$ ), we find that randomized versions of our defense can exhibit robust adversarial accuracies of  $\sim 70\%$  in comparison to  $0\%$  from the baseline.

## 4.1 Experimental Setup

We adopt the following settings to implement and evaluate our ensemble-based defense in detecting deepfakes and adversarial deepfakes.

**Datasets and Pre-processing.** We evaluate our defense using a dataset comprising GAN-generated images of individuals. Images are generated using the state-of-the-art StyleGAN [16], trained on the 128x128 FFHQ dataset of celebrity headshots. We use 50,000 images for training, 10,000 for validation, and 10,000 for testing sets. Finally, we transform all deepfake images to their frequency space representation using the 2D-DCT function, whereby pixel intensities are instead represented as a sum of cosine basis functions.

**DNN Architecture and Training.** All models in our ensembles implement the same shallow four-layer CNN employed by the baseline Frank et al.’s [5] frequency-space defense. Each model is individually trained by minimizing the binary cross-entropy loss with the Adam optimizer, using an initial learning rate of 0.001. We use a batch size of 512 for a maximum of 20 epochs (with early stopping based on AUC-ROC over the validation set). All models are trained using Madry-style adversarial training with PGD-10 attacks [30] on deepfake images. All models are implemented using the PyTorch v1.6.0 framework for Python.

**Ensemble Configurations.** We consider 3 configurations of our ensemble that partition frequency components (see Section 3.3) into 2, 4, or 8 disjoint subsets. These configurations allow for ensembles of *maximum* size  $n = 2, 4, 8$  respectively. For the remainder of this section, we refer to these configurations as  $S2, S4$  and  $S8$ . Consequently, we refer to the baseline Frank et al. [5] frequency-space classifier as  $S1$ , as it can be trivially viewed as an ensemble of size  $n = 1$ . For any given an ensemble of  $n$  models, the final decision is obtained via a voting function that computes the mean probability score (i.e., mean over all softmax scores output by the  $n$  models).

## 4.2 Results

### 4.2.1 Deepfake Detection Performance

We evaluate expected<sup>1</sup> classification AUC-ROC scores of  $S1$  (baseline), and of maximally sized  $S2, S4, S8$  ensembles on the testing set discussed in Section 4.1. We observe that all ensembles (even the  $S8$  ensemble in which each model only leverages 12.5% of input features) are able to achieve scores over 99%.

---

<sup>1</sup>Since basis partitioning as described in Section 3.3 is a randomized procedure, we presented mean and standard deviation results for all experiments.

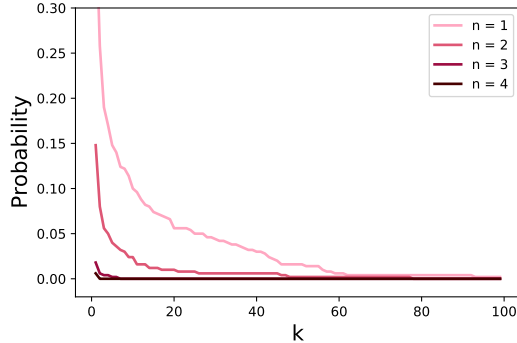


Figure 2: Probability of finding at least  $k$  orthogonal adversarial directions for  $\epsilon = 12/255$  for increasing ensemble sizes. Probabilities expectedly decrease as ensemble size increases. These results are for ensemble configuration  $S4$ .

We again emphasize the importance of selecting an appropriate basis for our partitioning scheme, in order to achieve these classification performances. We also compute scores obtained from ensembles that do not applying the 2D-DCT to images, i.e., for ensembles in the default pixel space. Each of these ensembles exhibit considerably lower performances of below 92%, as artifacts are not evenly distributed throughout the pixel space. We further visualize this in Figure 1 by examining the performance of individual models using increasingly small partitions of the pixel and frequency space. Models in the pixel space begin to suffer with smaller partitions, but models in the frequency space maintain a high performance.

#### 4.2.2 Dimensionality of Gradient-Aligned Adversarial Subspace

In section 3.1, we provide a result to estimate the dimensionality of the shared adversarial subspace for the  $L_2$  norm. In these experiments, we estimate the dimension for the  $L_\infty$  norm. Specifically, we use Tramer et al.’s [15] combinatorial construction to find  $k$  orthogonal vectors  $\mathbf{r}_1, \dots, \mathbf{r}_k$  satisfying  $\|\mathbf{r}_i\|_\infty = \epsilon$  and  $\mathbb{E}[\mathbf{g}^\top \mathbf{r}_i] \geq \epsilon \cdot \|\mathbf{g}\|_1 \cdot \frac{1}{\sqrt{k}}$  for all  $1 \leq i \leq k$ . Here,  $\mathbf{g}$  is the average of the individual model gradients.

The proposed method constructs orthogonal vectors by multiplying the row vectors from a Regular Hadamard matrix component-wise with  $\text{sign}(\mathbf{g})$ . For the baseline ( $S1$ ), and for each configuration ( $S1, S2, S4, S8$ ), we construct ensembles of varying sizes (upto maximums of  $n = \{1, 2, 4, 8\}$  respectively). We then select 1000 correctly classified inputs, and compute loss

gradients for each input. Using a regular Hadamard Matrix of order  $w$ , the above construction gives  $w$  orthogonal directions. Out of these  $w$ , the number of directions that are actually adversarial provide an estimate for  $k$ . We run the analysis for  $w \in \{4, 16, 36, 64, 100\}$ , and select the maximum value.

For configuration  $S4$ , Figure 2, plots the probability of finding at least  $k$  maximal orthogonal adversarial directions, as ensemble size increases. We observe that probability of finding these adversarial directions indeed decreases as ensemble size, i.e., number of orthogonal constraints increases. While not shown, these trends also hold for configurations  $S2, S8$ . Additionally, the expected value of maximum adversarial directions for maximally sized ensembles of all configurations ( $S2, S4, S8$ ) are 2, 0.5 and 0.006 respectively — these are all lower in comparison to 5 for the baseline  $S1$ .

Ensemble Type	PGD-100				Norm-PGD-100			
	Ensemble Size				Ensemble Size			
	1	2	4	8	1	2	4	8
$\epsilon = 2/255$								
S1	0.128 ± 0.000	-	-	-	0.124 ± 0.000	-	-	-
S2	0.966 ± 0.024	<b>1.000 ± 0.000</b>	-	-	0.970 ± 0.020	0.999 ± 0.002	-	-
S4	0.617 ± 0.172	0.999 ± 0.002	<b>1.000 ± 0.000</b>	-	0.597 ± 0.157	0.994 ± 0.005	<b>1.000 ± 0.000</b>	-
S8	0.039 ± 0.060	0.472 ± 0.170	0.738 ± 0.272	<b>1.000 ± 0.000</b>	0.052 ± 0.082	0.366 ± 0.184	0.586 ± 0.269	0.693 ± 0.208
$\epsilon = 4/255$								
S1	0.004 ± 0.000	-	-	-	0.012 ± 0.000	-	-	-
S2	0.236 ± 0.155	0.970 ± 0.027	-	-	0.246 ± 0.152	0.958 ± 0.040	-	-
S4	0.071 ± 0.159	0.874 ± 0.149	<b>1.000 ± 0.000</b>	-	0.074 ± 0.160	0.825 ± 0.194	<b>1.000 ± 0.000</b>	-
S8	0.004 ± 0.008	0.326 ± 0.154	0.613 ± 0.276	<b>1.000 ± 0.000</b>	0.005 ± 0.011	0.265 ± 0.311	0.586 ± 0.269	0.693 ± 0.208
$\epsilon = 8/255$								
S1	0.000 ± 0.000	-	-	-	0.000 ± 0.000	-	-	-
S2	0.000 ± 0.000	0.205 ± 0.185	-	-	0.000 ± 0.000	0.276 ± 0.181	-	-
S4	0.000 ± 0.000	0.027 ± 0.037	0.883 ± 0.121	-	0.000 ± 0.000	0.070 ± 0.115	<b>0.790 ± 0.232</b>	-
S8	0.000 ± 0.000	0.281 ± 0.273	0.450 ± 0.232	<b>1.000 ± 0.000</b>	0.000 ± 0.000	0.031 ± 0.070	0.168 ± 0.141	0.600 ± 0.193

Table 1: Adversarial accuracies of the baseline Frank et al. frequency space classifier ( $S1$ ) and our ensembles under PGD-100 and Norm-PGD-100 attacks at various  $\epsilon = \{2/255, 4/255, 8/255\}$ . For each of our ensemble configurations ( $S2, S4, S8$ ), we increase ensemble size from 1 upto the maximum (e.g., 8 models for  $S8$ ) to demonstrate the benefit of imposing additional orthogonal constraints on the adversary. Baseline and all ensemble models are adversarially trained on PGD-10 attacks.

### 4.2.3 Robustness Against Adversarial Examples

We evaluate robustness of  $S1$  (baseline), and our ensembles ( $S2, S3, S4$ ) against attacks in both the white-box and black-box settings. We follow prior

work on evaluating adversarial robustness [13] and employ *adversarial accuracy* (fraction of correctly classified adversarial examples) as our performance metric. A higher adversarial accuracy implies more robustness.

**White-Box PGD for Ensembles.** We begin by considering robustness under adversarial examples constructed by Madry et al.’s PGD attack algorithm. PGD is commonly accepted as a reliable first-order approach to discovering adversarial examples within an  $\epsilon$ -bounded  $L_\infty$ -ball around an input image [30]. Given image  $\mathbf{x}_0$  with true label  $y$ , PGD computes an adversarial example for classification ensemble  $E$  by (a) starting at a random point within the  $L_\infty$ -ball, and then (b) using projected gradient descent to iteratively move in the direction of the negative loss function  $\mathcal{L}_E$ :

$$\mathbf{x}_{t+1} = \text{clamp}(\mathbf{x}_t + \alpha * \text{sgn}(\nabla_x \mathcal{L}_E(\mathbf{x}_t, y)))$$

where  $\alpha$  is the step size for gradient descent, and the *clamp* operator clips values between  $[\mathbf{x}_0 - \epsilon, \mathbf{x}_0 + \epsilon]$ .

Recall from Section 4.1 that our ensembles output the mean of individual model softmax scores. We thus compute  $\nabla_x \mathcal{L}_E$  using this mean score to perform PGD attacks.

Ensemble Type	PGD-500				Norm-PGD-500			
	Ensemble Size				Ensemble Size			
	1	2	4	8	1	2	4	8
S1	0.000 ± 0.000	-	-	-	0.000 ± 0.000	-	-	-
S2	0.002 ± 0.002	0.519 ± 0.142	-	-	0.001 ± 0.002	0.234 ± 0.095	-	-
S4	0.000 ± 0.000	0.438 ± 0.178	<b>0.879 ± 0.032</b>	-	0.000 ± 0.000	0.014 ± 0.010	<b>0.265 ± 0.051</b>	-
S8	0.000 ± 0.000	0.000 ± 0.000	0.068 ± 0.054	0.553 ± 0.205	0.000 ± 0.000	0.000 ± 0.000	0.002 ± 0.004	0.012 ± 0.009

Table 2: Adversarial accuracies of the baseline Frank et al. frequency space classifier (S1) and our ensembles under more powerful PGD-500 and Norm-PGD-500 attacks with  $\epsilon = 1/255$ .

We first attack using PGD-100 for a variety of  $\epsilon \in \{2/255, 4/255, 8/255\}$  and follow Madry et al. [30] by initializing with  $\alpha = 0.25 * \epsilon$ . We perform a logarithmic search on  $\alpha$  and present adversarial accuracy for the optimal value. Results are presented in columns 2-5 of Table 1. All configurations of our ensembles demonstrate adversarial accuracies higher than S1. Furthermore, for any given configuration (S2, S4, S8), robustness increases with increase in ensemble size — this can be attributed to the additional orthogonal constraints corresponding to each additional model. This also follows from the analysis in Section 4.2.2, suggesting that reductions in adversarial subspace dimensionality are also reflected against a multi-step adversary. These trends hold consistent even against powerful PGD-500 attacks for  $\epsilon = 1/255$  (see columns 2-5 of Table 2).

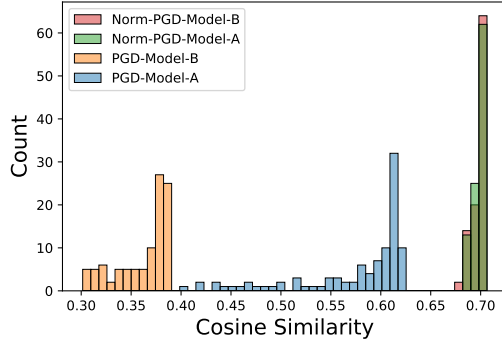


Figure 3: Cosine Similarity between the attack direction and gradient of losses of individual models for PGD-100 attack against  $S2$  model.

**White-box Norm-PGD for Ensembles.** Attacking an ensemble with PGD as described above may be viewed as equivalent to attacking with the average loss across all individual models. In fact, this is the de facto attack approach for evaluating adversarial robustness of ensembles [13]. However, this formulation for  $\mathcal{L}_E$  is subject to artifacts arising from large differences in gradient magnitudes across individual models. Specifically, if the  $j^{\text{th}}$  summand in  $\nabla_x \mathcal{L}_E$  has a dominating magnitude in comparison to others, then the averaged gradient’s direction is dominated by that model. This could cause PGD to “focus” more on attacking the  $j^{\text{th}}$  model. Consequently, other models could be neglected.

There exists an adjustment to  $\nabla_x \mathcal{L}_E$  that addresses this concern. Specifically, we observe that a sufficient condition for attack success is that *each* individual model is successfully attacked (this is because when each softmax score is below the decision threshold, so is the mean score). This may be viewed as a strategy from an attacker who aims to “focus” on each model equally during the attack. In this case, one can instead express  $\nabla_x \mathcal{L}_E$  as the mean of individual *normalized* model gradients, i.e.,  $\nabla_x \mathcal{L}_E = \frac{1}{n} \sum_{j=1}^n \frac{\nabla_x \mathcal{L}_{\mathcal{F}_j}}{\|\nabla_x \mathcal{L}_{\mathcal{F}_j}\|_2}$ .

We term this modification the Norm-PGD attack.

We repeat the attack settings from our above PGD evaluation, and present adversarial accuracies for our defense in columns 6-9 of Table 1. Our observations here are twofold. *First*, we note that Norm-PGD is expectedly a stronger attack against our ensembles than ordinary PGD — adversarial accuracy is reduced further than PGD under all attack settings. To visualize this phenomenon, we plot in Figure 3 the expected cosine similarities

between the final computed attack direction (i.e.,  $\nabla_x \mathcal{L}_E$ ) and individual model gradients for both the PGD-100 and Norm-PGD-100 attacks on  $S2$  ensembles of size  $n = 2$ . Under the PGD attack, it is clear that the final attack direction is more similar to one model’s gradient (blue bars) than the other (orange bars), confirming that it focuses on one model more than the other. However, the final attack direction is equally and highly similar to both models’ gradients (overlapping green and red bars) under Norm-PGD, suggesting that the imbalance has been addressed. *Second*, even though Norm-PGD is a stronger attack than PGD, we continue to observe the same trends in robustness, i.e., significantly more robustness than baseline  $S1$ , and increase in robustness as ensemble size increases.

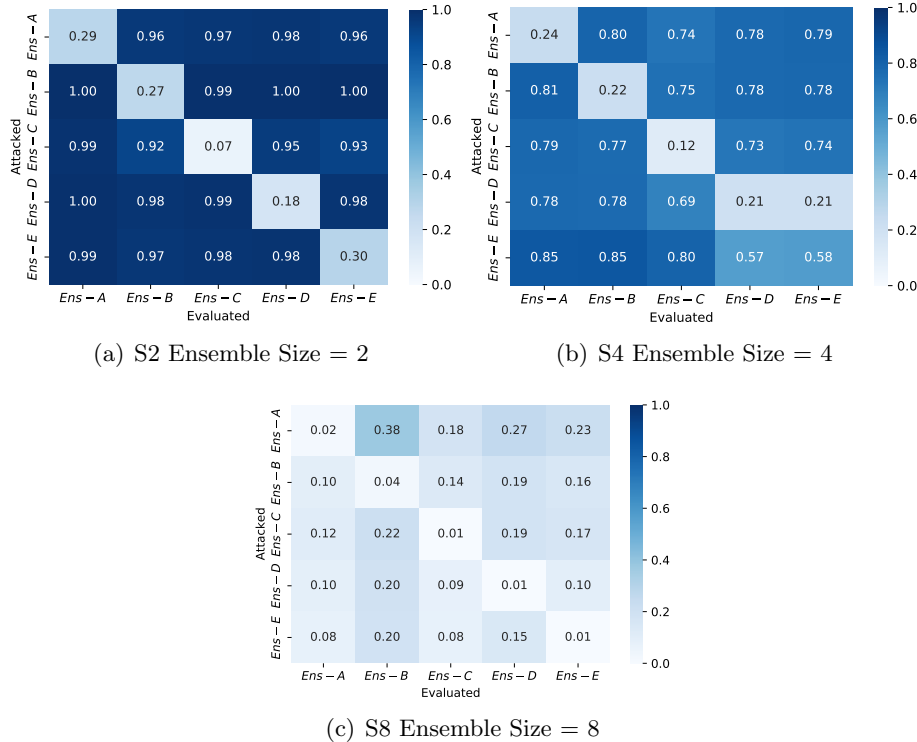


Figure 4: Transferability of PGD-500 with  $\epsilon = 1/255$  across 5 maximally sized ensembles for each configuration ( $S2$ ,  $S4$ ,  $S8$ ).

**Black-box Transfer Attacks.** We also evaluate robustness of our ensembles in the realistic black-box setting, in which the adversary has full knowledge of ensemble configuration (e.g.,  $S2$  or  $S4$ ) and size (e.g.,  $n = 3$ ),

but no access to internals of the ensemble i.e. the exact feature space partitioning. Here, the attacker can craft adversarial perturbations based on a surrogate ensemble of the same size (but with a different, randomly selected partitioning), and perform a *transfer attack*. Transfer attacks entail construction of white-box attacks against the adversary-controlled surrogate ensemble, and evaluating them against the defense ensemble.

For each ensemble configuration ( $S2, S4, S8$ ), we construct 5 ensembles of maximum size (and thus maximum robustness, see Tables 1 and 2), differing only in their input basis partitioning. We then (a) attack one of these ensembles using the white-box PGD-500 and Norm-PGD-500 attacks with  $\epsilon = 1/255$ , and (b) evaluate the strongest resulting adversarial examples (from either attack) against the remaining 4 ensembles. Results are presented in the matrices in Figure 4. We observe that  $S2$  ensembles exhibit almost no transferability (at worst 93% accuracy), and  $S8$  ensembles exhibit high transferability (at best 38% accuracy). This trend follows intuition — as one moves from the  $S2$  to the  $S8$  configuration and beyond, our partitioning scheme tends to yield “similar” ensembles. This is best understood by considering the hypothetical configuration of maximally sized “ $Sd$ ” ensembles, i.e., ensembles in which each of the  $d$  models operates on only a single frequency component. In this configuration, all 5 ensembles would be identical in their input basis partitioning, and would likely exhibit perfect transferability.

**Improving White-box Robustness with Randomization.** Existing defenses against adversarial examples have seen success in employing randomization, e.g., randomization over a collection of diverse transformations [31]. Such randomization forces the adversary to develop an attack that succeeds in expectation. This is typically achieved via Athalye et al.’s Expectation Over Transformation (EoT) strategy [32], in which gradients are averaged over the support of the random distribution. In these experiments, we investigate whether such randomization could further improve robustness of our ensembles.

As discussed in our black-box transferability analysis, for any given ensemble configuration and size we can construct multiple ensembles that differ in their input basis partitioning. Then, by performing inference using a randomly selected ensemble, we can force the adversary to optimize against a random distribution of, rather than deterministic set of orthogonal constraints.

To evaluate whether this “randomized pool of ensembles” strategy would improve robustness, we leverage the 5 maximally sized  $S2$  ensembles that exhibited minimum transferability, and attack them using EoT versions of PGD-500 and Norm-PGD-500 attacks. EoT versions of these attacks leverage

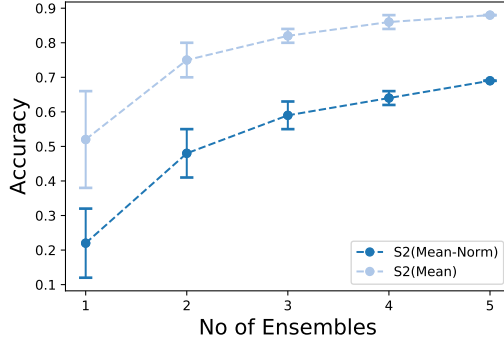


Figure 5: Adversarial accuracies for pools of  $\{1,2,3,4,5\}$  maximally sized  $S2$  ensembles ( $n = 2$ ) under EoT PGD-500 and EoT Norm-PGD-500 with  $\epsilon = 1/255$ .

gradients (or normalized gradients) averaged over all ensembles, rather than a single ensemble. For example, an EoT Norm-PGD attack against 5  $S2$  ensembles would set  $\nabla_x \mathcal{L}_E = \frac{1}{10} \sum_{i=1}^5 \sum_{j=1}^2 \frac{\nabla_x \mathcal{L}_{\mathcal{F}_{ij}}}{\|\nabla_x \mathcal{L}_{\mathcal{F}_{ij}}\|_2}$ , where  $\mathcal{F}_{ij}$  is the  $j^{th}$  model in the  $i^{th}$  ensemble.

We present results for an increasing pool size in Figure 5. We observe that randomization significantly improves robustness as pool size (i.e., the number of ensembles) increases, with improvements of upto  $\sim 70\%$  adversarial accuracy. This can be attributed to the low transferability between the  $S2$  ensembles. In other words, a randomized pool of ensembles constitutes a sufficiently diverse set of orthogonal constraints that complicates optimization for an adversary.

## 5 Conclusions

In this paper, we present an ensemble-based approach to deepfake detection that significantly improves adversarial robustness beyond standalone adversarial training. To this end, we characterize upper bounds on the dimension of the shared adversarial subspace in terms of model gradients. Inspired by these results, we construct ensembles of deepfake classifiers with pairwise orthogonal gradients induced by basis partitioning transformations, and show that such ensembles effectively reduce the attack surface. With the appropriately chosen DCT-induced basis, we empirically validate that

these ensembles exhibit near-perfect deepfake detection capabilities, while still offering significant robustness gains against a first-order adversary.

## 6 Acknowledgements

This work was supported by the DARPA GARD program under agreement number 885000. All opinions and findings are those of the authors and do not necessarily reflect the views of our research sponsors.

## References

- [1] Ian Goodfellow, Jean Pouget-Abadie, Mehdi Mirza, Bing Xu, David Warde-Farley, Sherjil Ozair, Aaron Courville, and Yoshua Bengio. Generative adversarial nets. *Advances in neural information processing systems*, 27, 2014.
- [2] Pierre Baldi. Autoencoders, unsupervised learning, and deep architectures. In *Proceedings of ICML workshop on unsupervised and transfer learning*, pages 37–49. JMLR Workshop and Conference Proceedings, 2012.
- [3] Paris Martineau. Facebook removes accounts with ai-generated profile photos. <https://www.wired.com/story/facebook-removes-accounts-ai-generated-photos/>, 2019.
- [4] Samantha Cole. Ai-assisted fake porn is here and we’re all f\*\*\*\*d. [https://www.vice.com/en\\_us/article/gydydm/gal-gadot-fake-ai-porn](https://www.vice.com/en_us/article/gydydm/gal-gadot-fake-ai-porn), 2017.
- [5] Joel Frank, Thorsten Eisenhofer, Lea Schönherr, Asja Fischer, Dorothea Kolossa, and Thorsten Holz. Leveraging frequency analysis for deep fake image recognition. In *International Conference on Machine Learning*, pages 3247–3258. PMLR, 2020.
- [6] Christian Szegedy, Wojciech Zaremba, Ilya Sutskever, Joan Bruna, Dumitru Erhan, Ian Goodfellow, and Rob Fergus. Intriguing properties of neural networks. In *International Conference on Learning Representations*, 2014.
- [7] Ian Goodfellow, Jonathon Shlens, and Christian Szegedy. Explaining and harnessing adversarial examples. In *International Conference on Learning Representations*, 2015.

- [8] Battista Biggio, Iginio Corona, Davide Maiorca, Blaine Nelson, Nedim Šrndić, Pavel Laskov, Giorgio Giacinto, and Fabio Roli. Evasion attacks against machine learning at test time. In *Joint European conference on machine learning and knowledge discovery in databases*, pages 387–402. Springer, 2013.
- [9] Nicholas Carlini and Hany Farid. Evading deepfake-image detectors with white-and black-box attacks. In *Proceedings of the IEEE/CVF Conference on Computer Vision and Pattern Recognition Workshops*, pages 658–659, 2020.
- [10] Paarth Neekhara, Brian Dolhansky, Joanna Bitton, and Cristian Canton Ferrer. Adversarial threats to deepfake detection: A practical perspective. In *Proceedings of the IEEE/CVF Conference on Computer Vision and Pattern Recognition*, pages 923–932, 2021.
- [11] Warren He, James Wei, Xinyun Chen, Nicholas Carlini, and Dawn Song. Adversarial example defense: Ensembles of weak defenses are not strong. In *11th {USENIX} workshop on offensive technologies ({WOOT} 17)*, 2017.
- [12] Sanjay Kariyappa and Moinuddin K Qureshi. Improving adversarial robustness of ensembles with diversity training. *arXiv preprint arXiv:1901.09981*, 2019.
- [13] Zhuolin Yang, Linyi Li, Xiaojun Xu, Shiliang Zuo, Qian Chen, Pan Zhou, Benjamin Rubinstein, Ce Zhang, and Bo Li. Trs: Transferability reduced ensemble via promoting gradient diversity and model smoothness. *Advances in Neural Information Processing Systems*, 34, 2021.
- [14] Florian Tramèr, Nicolas Papernot, Ian Goodfellow, Dan Boneh, and Patrick McDaniel. The space of transferable adversarial examples. *arXiv preprint arXiv:1704.03453*, 2017.
- [15] Florian Tramèr, Alexey Kurakin, Nicolas Papernot, Ian Goodfellow, Dan Boneh, and Patrick McDaniel. Ensemble adversarial training: Attacks and defenses. *arXiv preprint arXiv:1705.07204*, 2017.
- [16] Tero Karras, Samuli Laine, and Timo Aila. A style-based generator architecture for generative adversarial networks. In *Proceedings of the IEEE/CVF Conference on Computer Vision and Pattern Recognition*, pages 4401–4410, 2019.

- [17] Tero Karras, Timo Aila, Samuli Laine, and Jaakko Lehtinen. Progressive growing of gans for improved quality, stability, and variation. In *International Conference on Learning Representations*, 2018.
- [18] Andrew Brock, Jeff Donahue, and Karen Simonyan. Large scale gan training for high fidelity natural image synthesis. *arXiv preprint arXiv:1809.11096*, 2018.
- [19] Taesung Park, Ming-Yu Liu, Ting-Chun Wang, and Jun-Yan Zhu. Semantic image synthesis with spatially-adaptive normalization. In *Proceedings of the IEEE/CVF Conference on Computer Vision and Pattern Recognition*, pages 2337–2346, 2019.
- [20] Jun-Yan Zhu, Taesung Park, Phillip Isola, and Alexei A Efros. Unpaired image-to-image translation using cycle-consistent adversarial networks. In *Proceedings of the IEEE international conference on computer vision*, pages 2223–2232, 2017.
- [21] Yunjey Choi, Minje Choi, Munyoung Kim, Jung-Woo Ha, Sunghun Kim, and Jaegul Choo. Stargan: Unified generative adversarial networks for multi-domain image-to-image translation. In *Proceedings of the IEEE conference on computer vision and pattern recognition*, pages 8789–8797, 2018.
- [22] Sheng-Yu Wang, Oliver Wang, Richard Zhang, Andrew Owens, and Alexei A Efros. Cnn-generated images are surprisingly easy to spot... for now. In *Proceedings of the IEEE/CVF Conference on Computer Vision and Pattern Recognition*, pages 8695–8704, 2020.
- [23] Ning Yu, Larry S Davis, and Mario Fritz. Attributing fake images to gans: Learning and analyzing gan fingerprints. In *Proceedings of the IEEE/CVF International Conference on Computer Vision*, pages 7556–7566, 2019.
- [24] Scott McCloskey and Michael Albright. Detecting gan-generated imagery using color cues. *arXiv preprint arXiv:1812.08247*, 2018.
- [25] Lakshmanan Nataraj, Tajuddin Manhar Mohammed, BS Manjunath, Shivkumar Chandrasekaran, Arjuna Flenner, Jawadul H Bappy, and Amit K Roy-Chowdhury. Detecting gan generated fake images using co-occurrence matrices. *Electronic Imaging*, 2019(5):532–1, 2019.

- [26] Xu Zhang, Svebor Karaman, and Shih-Fu Chang. Detecting and simulating artifacts in gan fake images. In *2019 IEEE International Workshop on Information Forensics and Security (WIFS)*, pages 1–6. IEEE, 2019.
- [27] Ricard Durall, Margret Keuper, Franz-Josef Pfreundt, and Janis Keuper. Unmasking deepfakes with simple features. *arXiv preprint arXiv:1911.00686*, 2019.
- [28] Seyed-Mohsen Moosavi-Dezfooli, Alhussein Fawzi, Omar Fawzi, and Pascal Frossard. Universal adversarial perturbations. In *Proceedings of the IEEE conference on computer vision and pattern recognition*, pages 1765–1773, 2017.
- [29] Dongxian Wu, Yisen Wang, Shu-Tao Xia, James Bailey, and Xingjun Ma. Skip connections matter: On the transferability of adversarial examples generated with resnets. *arXiv preprint arXiv:2002.05990*, 2020.
- [30] Aleksander Madry, Aleksandar Makelov, Ludwig Schmidt, Dimitris Tsipras, and Adrian Vladu. Towards deep learning models resistant to adversarial attacks. In *International Conference on Learning Representations*, 2018.
- [31] Edward Raff, Jared Sylvester, Steven Forsyth, and Mark McLean. Barrage of random transforms for adversarially robust defense. In *Proceedings of the IEEE/CVF Conference on Computer Vision and Pattern Recognition*, pages 6528–6537, 2019.
- [32] Anish Athalye, Logan Engstrom, Andrew Ilyas, and Kevin Kwok. Synthesizing robust adversarial examples. In *Proc. of ICML*, 2018.

## A Proofs

### A.1 Proof of lemma 3.1

Given  $n$  models,  $\mathcal{F}_1, \dots, \mathcal{F}_n$ , having gradients  $\mathbf{g}_1, \dots, \mathbf{g}_n \in \mathbb{R}^d$  for input-label pair  $(\mathbf{x}, y)$  (where  $\mathbf{g}_j = \nabla_{\mathbf{x}} \mathcal{L}_{\mathcal{F}_j}(\mathbf{x}, y)$ ), the maximum number  $k$  of orthogonal vectors  $\mathbf{r}_1, \mathbf{r}_2, \dots, \mathbf{r}_k \in \mathbb{R}^d$  satisfying  $\|\mathbf{r}_i\|_2 \leq \epsilon$  and  $\mathbf{r}_i^\top \mathbf{g}_j \geq \gamma_j$  for all  $1 \leq i \leq k$  and  $1 \leq j \leq n$  is given by:

$$k \leq \min(k_{ind}, k_{sim}, d)$$

where,  $k_{ind} = \min_{1 \leq j \leq n} \frac{\epsilon^2}{\gamma_j^2} \|\mathbf{g}_j\|_2^2$

$$k_{sim} = \frac{\epsilon^2}{\left(\sum_{j=1}^n \gamma_j\right)^2} \left( \sum_{j=1}^n \|\mathbf{g}_j\|_2^2 + \sum_{j_1=1}^n \sum_{j_2=1}^n \mathbf{g}_{j_1}^\top \mathbf{g}_{j_2} \right)$$

Proof:

Since,  $\mathbf{r}_1, \mathbf{r}_2, \dots, \mathbf{r}_k$  are orthogonal, we have

$$\begin{aligned} \left\| \sum_{j=1}^n \mathbf{g}_j \right\|^2 &\geq \sum_{i=1}^k \left| \left( \sum_{j=1}^n \mathbf{g}_j \right)^\top \hat{\mathbf{r}}_i \right|^2 \\ &\geq \sum_{i=1}^k \frac{\left| \left( \sum_{j=1}^n \mathbf{g}_j \right)^\top \mathbf{r}_i \right|^2}{\|\mathbf{r}_i\|_2^2} \\ &\geq \frac{1}{\epsilon^2} \sum_{i=1}^k \left| \left( \sum_{j=1}^n \mathbf{g}_j \right)^\top \mathbf{r}_i \right|^2 \\ &\geq \frac{1}{\epsilon^2} k \left( \sum_{j=1}^n \gamma_j \right)^2 \end{aligned}$$